Available online at www.sciencedirect.com
ScienceDirect
Journal of Nuclear Materials 363–365 (2007) 723–727
journal of nuclear materials
www.elsevier.com/locate/jnucmat

Stochastic boundary modeling by resonant magnetic perturbations on DIII-D

L.W. Yan [a], T.E. Evans [b,*]

[a] Southwestern Institute of Physics, P.O. Box 432, Chengdu, Sichuan, China
[b] General Atomics, P.O. Box 85608, San Diego, CA 92186-5608, USA

Abstract

A 3-D field line integration code (TRIP3D) is used to trace stochastic field lines in the edge of DIII-D plasmas in which edge localized modes (ELMs) are suppressed by resonant magnetic perturbations (RMPs). In these experiments normalized RMPs of 2.6×10^{-4} on the 95% flux surface produce complete ELM suppression, while global confinement stays high. The particle and heat diffusion coefficients produced by stochastic magnetic field on 95% flux surface have been calculated without and with ELM suppression. They are different from experimental results. The reason is that stochastic quasi-linear diffusion theory cannot be applied for the experimental explanation due to the complex nature of the transport physics involved when boundary layer field lines connect regions of hot plasma directly to material surfaces.

PACS: 52.65.Cc; 52.55.Fa; 52.25.Fi

Keywords: DIII-D; Edge modeling; ELM; Magnetic topology; Stochastic boundary

1. Introduction

H-mode discharges with high edge pressure gradients are expected to be required for the economic feasibility of future fusion reactors. However, the high edge pressure gradients easily produce an ELM instability [1], which expels large heat and particle loading to the divertor targets. These ELMs limit the core plasma performance and reduce the lifetime of divertor target plates. The transport of heat and particles outward across the plasma boundary is useful to control density and impurity profiles for steady-state, high-performance operations. Consequently, any technique to eliminate or mitigate large fast ELM impulses must replace the transient heat and particle transport with another quasi-steady transport process. Such a technique is high priority for a burning plasma device such as ITER [2].

Recently, several methods have been found to avoid large ELMs. The quiescent H-mode (QH-mode) is a type of high performance discharge, without large ELMs discovered on DIII-D and reproduced in other devices [3]. The enhanced D_α (EDA) H-mode without ELMs, obtained in Alcator C-Mod, depends on a quasi-coherent MHD mode

* Corresponding author.
E-mail addresses: lwyan@swip.ac.cn (L.W. Yan), evans@fusion.gat.com (T.E. Evans).

0022-3115/$ - see front matter © 2007 Elsevier B.V. All rights reserved.
doi:10.1016/j.jnucmat.2007.01.192

near the separatrix for particle control [4]. Another H-mode scenario without large ELMs is high recycling steady (HRS) H-mode observed in JFT-2M [5]. Recent experiments in DIII-D indicate that static RMPs can effectively decrease or eliminate large, fast ELMs without degrading confinement performance [6,7]. This suppression depends on the magnetic perturbation amplitude, safety factor, heating power and plasma density. A 3-D code is used to model stochastic boundaries on DIII-D [8], ergodic divertor on Tore Supra [9], dynamic ergodic divertor on TEXTOR [10].

2. Experimental results of large ELM suppression

Steady-state H-mode plasmas without large ELMs have been achieved in the DIII-D tokamak by applying small RMPs [7]. In these experiments, a normalized radial magnetic perturbation of 2.6×10^{-4} [11] on the 95% flux surface ($\psi_N = 0.95$) produces complete ELM suppression, while global confinement stays high. A typical example is discharge 123301 with an $n = 3$ even-parity I-coil current of $I_c = 3.3$ kA t and an $n = 1$ C-coil current of 12 kA t. Main parameters at $t = 3$ s are $R = 1.65$ m, $a = 0.6$ m, $B_t = -2.0$ T, $I_p = 1.5$ MA, safety factor $q_{95} = 3.7$. In discharge 123301 both the single turn I-coil, located inside the vacuum vessel, and the four-turn C-coil located outside the vacuum vessel are used to completely eliminate ELMs, while in discharge 123302 with the C-coil but without the I-coil the ELMs are not suppressed. The edge profiles of electron temperature and density for two discharges are given in the Fig. 8 of Ref. [11]. An increase in the divertor CIII emission in discharge 123301 suggests that particles from inside the magnetic separatrix directly reach divertor plates across a stochastic boundary with the I-coil RMP. This increase in CIII is not seen in discharge 123302 without the I-coil RMP. The H-factor and normalized beta increase slightly in ELM suppressed discharges compared to those without ELM suppression. Here, we model the magnetic field line structure of discharge 123301 and 123302 and compare the changes due to the I-coil RMP.

3. The modeling of stochastic field transport

A 3-D field line integration code, TRIP3D, was developed to model RMPs in poloidally diverted tokamaks [12]. In TRIP3D, the unperturbed magnetic field (B_R, B_ϕ, B_Z) at each point is provided by the EFIT code [13]. The perturbed field (b_R, b_ϕ, b_Z), produced by I-coil and C-coil currents as well as error fields, is calculated for each integration step and added to the unperturbed axisymmetric EFIT field. The code integrates a set of first-order cylindrical (R, ϕ, Z) magnetic differential equations given as [14]

$$\frac{\partial R}{\partial \phi} = \frac{R(B_R + b_R)}{B_\phi + b_\phi}, \quad \frac{\partial Z}{\partial \phi} = \frac{R(B_Z + b_Z)}{B_\phi + b_\phi}. \tag{1}$$

The diffusion coefficient that can be calculated in TRIP3D and is representative of the stochasticity of a field line is defined as, $D_{st} = \delta r^2/2L$, where δr is the radial random step between the flux surfaces at the outboard midplane and L is the field line length. Here, L is taken in the limit of 200 toroidal revolutions or when the field line hits a material surface such as a divertor target plate. The diffusion coefficient in flux space, $\left\langle D_{st}^{\psi} \right\rangle = \frac{1}{M}\sum_{i=1}^{M} \delta\psi_i^2/2L_i$, is applied to the $\langle D_{st}\rangle$ calculation. The two coefficients are related by $\langle D_{st}\rangle = C^2 r^2 \langle D_{st}^{\psi}\rangle/4\psi_i^2$. The coordinate conversion coefficient is $C = 1.03$–1.27 for the DIII-D discharges. $C = 1.25$ is a reasonable approximation for edge plasma. The radial particle diffusion coefficient is calculated using $D_m = \langle D_{st}\rangle \times C_s$, where $C_s = \sqrt{(T_e + T_i)/m_i}$ is the ion acoustic speed. In contrast, collisionless electron conductivity is defined as [15], $\chi_e = \langle D_{st}\rangle \times v_{T_e}$, where $v_{T_e} = \sqrt{T_e/m_e}$ is thermal electron speed.

4. Calculation results for ELM suppression in DIII-D

Fig. 1 shows a Poincaré plot of the field line positions for normalized magnetic flux versus poloidal angle for shot 123301 at $t = 3.0$ s with complete ELM suppression. Here, 72 uniformly distributed field lines are followed on each flux surface starting at $\psi_N = 0.7$ and ending at $\psi_N = 1.0$ with the step of $\Delta\psi_N = 0.05$. Each field line is preset for a maximum of 200 toroidal revolutions that results in a maximum length of about 2000 m or roughly of order a collisional electron mean free path (L_c). For example, using $T_{e,95} = 1.2$ keV, $n_{e,95} = 1.3\times10^{19}$ m^{-3}, we find $L_{c,95} = 942$ m at $\psi_N = 0.95$. The large $m/n = 2/1$ magnetic island seen at $\psi_N = 0.67$ has a width $\Delta\psi_N = 0.06$ and results from the C-coil which is configured to correct $n = 1$ field-errors in these experiments. The C-coil also produces an $m/n = 3/1$ island chain on the $\psi_N = 0.88$ surface with a width $\Delta\psi_N = 0.025$. It should be noted that there

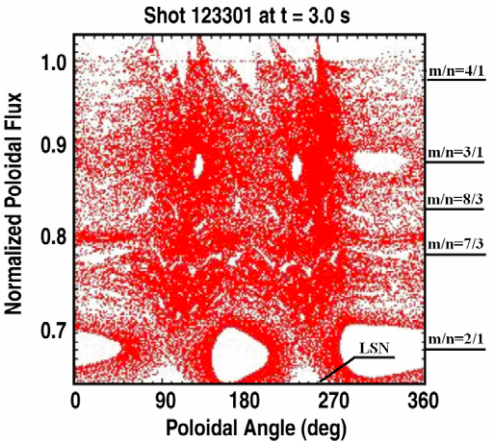

Fig. 1. Poincaré plot of the field line positions for normalized magnetic flux versus poloidal angle in shot 123301 at $t = 3$ s with complete ELM suppression.

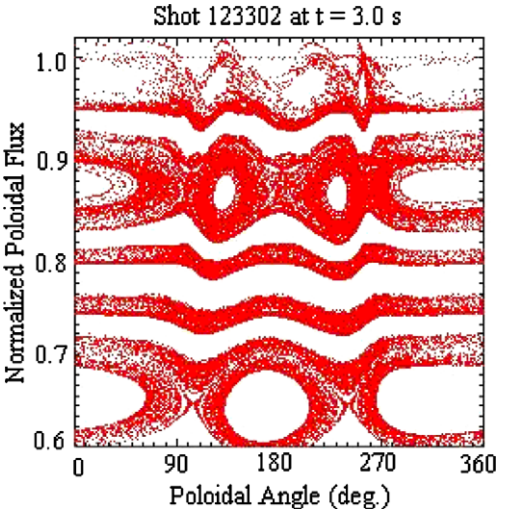

Fig. 2. Pioncaré plot of the field line positions for normalized magnetic flux versus poloidal angle in shot 123302 at $t = 3$ s without ELM suppression.

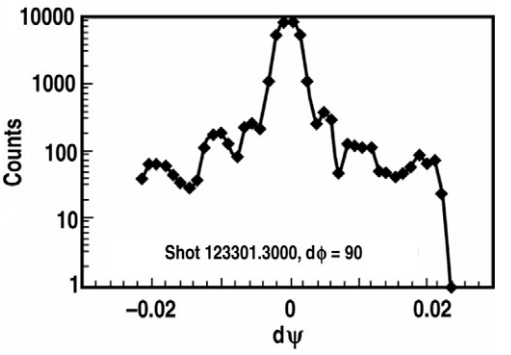

Fig. 3. Counts versus the flux steps within toroidal angle of 90° for shot 123301 at $t = 3.0$ s.

are also small islands between $\psi_N = 0.78$ ($m/n = 7/3$) and $\psi_N = 0.84$ ($m/n = 8/3$) are produced by the $n = 3$ I-coil perturbations and field-errors from 18 PF and 24 TF coils. Field line dots occupy almost entire space except island regions even with the step of $\Delta\psi_N = 0.05$. The combined I-coil, C-coil and field-error perturbations produce a relatively strong stochastic boundary region in these plasmas and field lines begin to connect to the divertor targets in less than 200 revolutions once $\psi_N > 0.80$. This relatively strong stochasticity also reduces the islands widths. All of the open field lines eventually hit the lower divertor in this lower single null (LSN) discharge. There are four stripe-like features between 80° and 250° on the top near $\psi_N = 1.0$, which are consistent with the Hamiltonian structure of the system and a splitting of the separatrix into two invariant manifolds [16,17] (only one of which is seen because the field lines in this figure are all integrated in one direction from the starting point). Here, the edge safety factor is larger than 4 and coincides with the four stripe-like features defined by one of the invariant manifolds. Note that the density of field line intersections with the Pioncaré plane is higher between 90° and 270° indicating that the field lines have more probability appearing in the HFS than in the LFS. In discharge 123302, with the C-coil and field-errors but no I-coil, the stochasticity is significantly weaker and wider magnetic islands are observed, as shown in Fig. 2.

Fig. 3 shows the distribution of radial flux steps $\delta\psi_N$ found after integrating through a toroidal angle $\Delta\phi = 90°$ in the I-coil on discharge 123301 at time $t = 3.0$ s starting from $\psi_N = 0.95$. The maximum step with the I-coil is $\delta\psi_N = 2.4\%$, which often appears just before the field lines hit the divertor targets. Most steps are $\delta\psi_N \leqslant 0.29\%$. The relatively good symmetry of distribution about $\delta\psi_N = 0$ indicates that many toroidal revolutions of the field lines are needed before being lost to the divertor targets. The maximum count is 8451 with $\delta\psi_N = -0.058\%$. The wings of the distribution are dominated by near field interactions as the field lines pass through regions close to the I-coil. Large magnetic islands produce an additional degree of complexity in the distribution since the trajectories can become very chaotic near the islands.

The maximum flux step size ($\delta\psi_N$) with the I-coil off decreases to $\delta\psi_N = 1.65\%$, and is dominated by

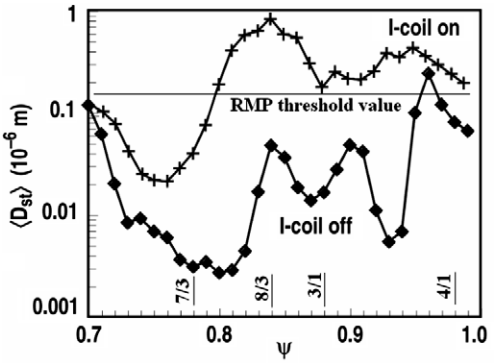

Fig. 4. Magnetically perturbed diffusion coefficient versus normalized flux for shot 123301 and 123302.

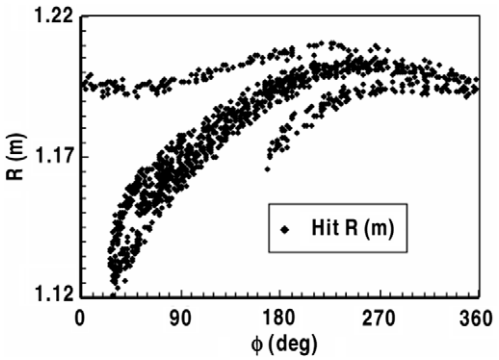

Fig. 5. Major radius of hit points versus toroidal angle for shot 123301.

the $m/n = 4/1$ magnetic island shown in Fig. 2. The step size difference of short path integrals ($\Delta\phi = 90°$) with or without ELM suppressions is not very large. Calculations of the field line properties using long path integrals ($\Delta\phi \gg 90°$) is expected to be related to a global magnetic diffusion coefficient of the system since local effects are reduced.

Fig. 4 shows the stochastic magnetic diffusion coefficient $\langle D_{st}\rangle$ versus normalized flux for a discharge with the I-coil (upper) and without one (lower). Here, 180 field lines are traced on each flux surface and the flux step $\Delta\psi_N$ between each surface is 0.01. As seen in Fig. 4, the edge magnetic diffusion coefficient with the I-coil tends to decrease with normalized magnetic flux for $\psi_N > 0.84$. The stochastic magnetic field line diffusion coefficient at $\psi_N = 0.95$ is $\langle D_{st}\rangle = 4.6 \times 10^{-7}$ m. Based on this, the radial particle diffusion coefficient is $D_m = 0.29$ m^2/s using ion acoustic speed $C_s = 6.3 \times 10^5$ m/s by $T_{e,95} = 1.2$ keV and $T_{i,95} = 3$ keV, while collisionless electron conductivity is $\chi_e = 6.7$ m^2/s. Therefore, the edge diffusion appears to be dominated by stochastic magnetic field after large ELM suppression. Results from TRIP3D also show that the field line length abruptly drops in edge region because of field lines lost on divertor targets, with lengths of 1976 m at $\psi_N = 0.7$, 1124 m at $\psi_N = 0.95$ and 497 m at $\psi_N = 0.99$.

The magnetically perturbed diffusion coefficient in the discharge without the I-coil perturbation field is well below that in the discharge with the I-coil perturbation field. Here, the particle radial diffusion coefficient is $D_m = 0.046$ m^2/s using $C_s = 4.6 \times 10^5$ m/s by $T_{e,95} = 0.9$ keV and $T_{i,95} = 1.3$ keV, while collisionless electron conductivity is $\chi_e = 1.25$ m^2/s. This level of stochasticity is apparently insufficient to suppress the large ELMs. It is found that changes caused by the magnetic perturbations in the pedestal profiles cannot be explained by a straightforward application of stochastic quasi-linear diffusion theory due to the complex nature of the transport physics involved when boundary layer field lines connect regions of hot plasma directly to material surfaces [18,19].

Fig. 5 shows the radial variation in field line hit points for discharge 123301 with the I-coil currents versus toroidal angle on the lower divertor targets which are located near poloidal angle 250° in these LSN diverted discharges, as shown in Fig. 1. The hit profile is asymmetric along toroidal direction dependent on the asymmetry of I-coil currents. The hit width is 1.5–7.0 cm and there are three clear stripes indicating that the toroidal mode of I-coil currents ($n = 3$) is determining the structure of the field line hit pattern on the divertor targets [8]. This pattern is consistent with lobes from an invariant manifold intersecting the divertor targets when the separatrix is split by the $n = 3$ I-coil perturbation [16]. The maximum width of the field line hit pattern in the 123302 discharge without the I-coil drops to 4 cm and the pattern changes to that of a single stripe. In addition, fewer field lines hit the divertor plates in the discharge without the I-coil because of the weaker stochastic field produced by DIII-D field errors. The broader radial profile of hit points in the discharge with the I-coil is expected to spread the heat load on the divertor but, at the same time, more field lines from the region of the pedestal plasma hit the divertor targets. Images of the divertor using IR data for the discharge modeled here do not show evidence of heat flux spreading during the I-coil perturbation, although in other discharges

using the I-coil, a splitting of the heat flux is observed [17].

5. Conclusions

Large ELMs have been completely suppressed in DIII-D using stochastic magnetic boundary provided by I-coil and C-coil currents. The radial magnetic perturbation is increased in discharges with ELM suppression, while global confinement stays high. The 3-D TRIP3D modeling gives the radial particle diffusion coefficients produced by stochastic field on flux surface $\psi_N = 0.95$ as 0.29 m^2/s with full ELM suppression and 0.046 m^2/s without ELM suppression, the corresponding collisionless electron conductivities are 6.7 m^2/s and 1.25 m^2/s. Stochastic quasi-linear theory cannot be directly applied to the experimental explanation because of complex boundary transport process, while edge electron temperature predicted by TRIP3D/E3D code is also smaller than the measured value [8]. Modeling indicates that the field line hit pattern on the divertor target plates in discharges with ELM suppression have an $n = 3$ toroidal asymmetry due to the $n = 3$ I-coil perturbation field and a radial width of 1.5–7.0 cm, which is consistent with the observation by tangential TV images [8].

Acknowledgements

This work was supported in part by the US Department of Energy under DE-FC02-04ER54698, DE-AC02-76CH03073 and DE-AC05-00OR22725 and by the Chinese Ministry of Science and Technology under 001CB710904 through the fusion collaboration between China and USA on fluid plasma simulation. We would like to thank Dr C. Wong of General Atomics for arranging the collaboration.

References

[1] A. Loarte, M. Becoulet, G. Saibene, et al., Plasma Phys. Control. Fus. 44 (2002) 1815.
[2] ITER Physics Basis, Nucl. Fusion 39 (1999) 2137.
[3] C.M. Greenfield, K.H. Burrell, J.C. DeBoo, et al., Phys. Rev. Lett. 86 (2001) 4544.
[4] J.E. Rice, P.T. Bonoli, E.S. Marmar, et al., Nucl. Fusion 42 (2002) 510.
[5] K. Kamiya, H. Kimura, H. Ugawa, et al., Nucl. Fusion 43 (2003) 1214.
[6] T.E. Evans, R.A. Moyer, P.R. Thomas, et al., Phys. Rev. Lett. 92 (2004) 2350003-1.
[7] K.H. Burrell, T.E. Evans, E.J. Doyle, et al., Plasma Phys. Control. Fus 47 (2005) B37.
[8] I. Joseph, R.A. Moyer, T.E. Evans, et al., these proceedings.
[9] Ph. Ghendrih, M. Bécoulet, L. Colas, et al., Nucl. Fusion 42 (2002) 1221.
[10] S.S. Abdullaev, K.H. Finken, M. Jakubowski, M. Lenhnen, Nucl. Fusion 46 (2006) S113.
[11] T.E. Evans, K.H. Burrell, M.E. Fenstermacher, et al., Phys. Plasmas 13 (2006) 056121.
[12] T.E. Evans, R.A. Moyer, P. Monat, Phys. Plasmas 9 (2002) 4957.
[13] L. Lao, R.H. St. John, R.D. Stambaugh, et al., Nucl. Fusion 25 (1985) 1611.
[14] Longwen Yan, T.E. Evans, S.M. Kaye, R. Maingi, Nucl. Fusion 46 (2006) 858.
[15] A.B. Rechester, M.N. Rosenbluth, Phys. Rev. Lett. 40 (1978) 38.
[16] R.K.W. Roeder, B.I. Rapoport, T.E. Evans, Phys. Plasmas 10 (2003) 3796.
[17] T.E. Evans, R.K.W. Roeder, J.A. Carter, et al., J. Phys.: Conf. Ser. 7 (2005) 174.
[18] Ph. Ghendrih, A. Grosman, H. Capes, Plasma Phys. Control. Fus 38 (1996) 1653.
[19] P.C. Stangeby, The plasma Boundary of Magnetic Fusion Devices, Plasma Physics Series, IOP Publishing Ltd., 2000.